Rec'd January 10, 1974

A SEARCH FOR CONTINUOUS FLUORESCENCE IN REFLECTION NEBULAE

NGR-36-010-016
Univ. of Toledo

DRB

William F. Rush* and Adolf N. Witt†

Ritter Astrophysical Research Center
The University of Toledo
Toledo, Ohio 43606

Received: _____

*Visiting Student, Kitt Peak National Observatory, which is operated by the Association of Universities for Research in Astronomy, Inc., under contract with the National Science Foundation.

†Visiting Astronomer, Kitt Peak National Observatory, which is operated by the Association of Universities for Research in Astronomy, Inc., under contract with the National Science Foundation.

ABSTRACT

Photometric and spectrophotometric observations have been made of the reflection nebulae NGC1435, NGC2068, NGC7023, and IC1287 in an attempt to detect continuous fluorescence by dust grains. Several effects of importance for observations of such faint objects are discussed, including instrumental light scattering, a photographic effect, and a time delay effect which can occur if the illuminating star is a spectrum variable. It is found that continuous fluorescence by interstellar grains is not likely to exist and that it cannot account for more than 10 percent of the total surface brightness of these reflection nebulae. No evidence of diffuse interstellar features is found in the spectra of these nebulae.

I. Introduction

The high surface brightness of reflection nebulae has led to suggestions that fluorescent processes may occur in such objects. Such suggestions have been made by Aller (1955) and by Struve and Swings (1948). The possibility of fluorescence in particular matter composing reflection nebulae is also suggested by the observation that many minerals fluoresce under ultraviolet light and/or particle bombardment, as shown by Blair and Edgington (1968). They report that fluorescence is often enhanced at low temperatures. Spectra discussed by Becker (1969) indicate that many organic molecules fluoresce under ultraviolet excitation. Such molecules frequently have quite broad emission features, and are possible constituents of the interstellar medium.

These considerations prompted the undertaking of a program of photometric and spectrophotometric observations of reflection nebulae in order to search for possible fluorescence. The two types of observations are complementary in the sense that the photographic spectrophotometry can detect fluorescence at many wavelengths simultaneously and is sensitive to discrete emission features, while the photoelectric photometry to be described is not limited by non-linear photographic effects at low intensities.

It should be remarked at the outset that if fluorescence is indeed present in reflection nebulae, it would not be expected to appear as a discrete line or broad (50-100Å) emission feature. Many previous observers have obtained spectrograms of reflection nebulae and would certainly have

detected any such emission. What may have escaped detection, however, is the existence of continuous fluorescence in which the fluorescent contribution to surface brightness is nearly the same for a broad wavelength range.

The presence of a fluorescent contribution to the surface brightness can be detected with either the photographic or photoelectric observations by essentially the same technique. In general, the presence of continuous fluorescence can be detected by comparing the depth of an absorption feature in the reflected spectrum to the depth of the same feature in the illuminating star. Fluorescence of intensity Φ manifests itself by the reflected lines appearing less deep than the corresponding lines in the illuminating star as shown in Figure 1. Here Φ is measured in units of the reflected continuum flux. This technique is known as the method of line depth and is discussed in more detail by Grainger and Ring (1961) and Link (1961).

II. The Photographic Observations

The photographic spectrophotometric observations were conducted on the 84-inch (2.1m) reflection telescope of the Kitt Peak National Observatory. The Carnegie-image-tube spectrograph was employed with a grating having 600 gr/mm, blazed for 4000Å in first order and having a dispersion of 130Å/mm. No filter was used in conjunction with the Kodak IIa-O Spectroscopic Plates. These plates were developed for 15 minutes at 68°F in D-76 developer and were calibrated with the spot sensitometer of the 84-inch telescope. The projected slit length for nebular exposures was 270". Observations were made during the periods September 27 to 29, 1970 and December 29 to 31, 1970. See Table I for details.

Each observation consisted of an exposure of the illuminating star, followed by an exposure of a nearby dark sky area, an exposure of the nebula, another exposure of the sky, and another observation of the star. Each of the sky exposures was as long as the nebular exposure. The nebulae which were studied were NGC 1435, NGC 2068, and NGC 7023.

As a control, observations were made in which the light scattered in the atmosphere and instrument was observed and treated as if it were nebular light. These observations were usually made on hazy nights. Control stars were 15 Sextantis, ζ^2 Ceti, and i Aquilae.

The spectrograms were reduced by use of the Gaertner digital microphotometer of the Yerkes Observatory. Scans were made of all spectra, including sky, nebular, and stellar spectra and the clear plate beside each spectrogram and the densities thus obtained were converted to punched cards. Plate background densities were removed by averaging the clear plate scans and point by point subtracting this average from the observed densities. In order to convert density into intensity, the 13 spots of

known relative intensity produced by the sensitometer for each night were plotted on a density-intensity curve and the photographic characteristic curve was fitted in three separate regions with a second order polynomial. The transitions between the three regions were chosen so that the characteristic curve and its derivative were smooth. The sky contributions to the nebular spectra were removed by averaging the sky spectrum taken before the nebular observation with the sky spectrum taken after the nebular observation. The accuracy with which one spectrum could be aligned with another was ±1.3Å. In order to reduce the noise level, all spectra of the same nebula were then aligned and averaged, point by point. All spectra of the same star were then also averaged. The averaged stellar and nebular spectra were then aligned and the ratio

$$(1) \qquad R(\lambda) = \frac{I_{Neb}(\lambda)}{I_{*}(\lambda)}$$

was computed point by point. Here the subscripts Neb and * indicate that the corresponding intensities are nebular and stellar. The ratio R was then plotted as a function of λ. Note that if only reflection processes are operative in a reflection nebula, the plot of $R(\lambda)$ against λ should be a smooth line. Continuous fluorescence manifests itself by producing a peak in the $R(\lambda)$ plot at the position of strong absorption lines, since the nebular line appears to be filled in by the fluorescence.

III. Results of the Photographic Observations

A typical final plot of the reduced observations is shown in Figure 2 for NGC1435. Other nebulae showed similar results with virtually identical dependence of R on wavelength. The only exception to this is NGC7023, discussed below. However, the scattered light control observations produced very similar plots of R as a function of λ, a fact which

indicates that the apparent fluorescence of Figure 2 is actually an instrumental effect.

The origin of this effect can be recognized from Figure 3. With increasing distances, r, from the illuminating star, the nebular surface brightness generally decreases. Both the line and continuum intensities are shown decreasing with linear gradients, but the effect operates with any gradient (see Figure 3b). Shown in Figure 3a is the photographic characteristic curve relating intensity and density; the toe of the curve is the key to the effect being discussed. In Figure 3c we see the density of the photographic plate after the spectrum has been taken. The continuum is still linear (or has the same shape that it originally had) because its higher intensity places it in the linear region of the characteristic curve so that the transformation or mapping from log I to D, the density, is linear. However, at the lower intensity at which the line center is being exposed, this transformation from log I to D is nonlinear, resulting in a distortion of the type shown schematically in Figure 3c. The averaging action of the scanning slit of the microphotometer will indicate a density in the line corresponding to a smaller value of r than it will for the continuum in this case. To see this, note that the centroid for the "line" curve in Figure 3c is to the left of the centroid of the "continuum curve." This creates the false impression that the lines are "filled."

Although it is difficult to quantitatively determine the magnitude of this effect, the fact that the control results appear to be substantially the same as the nebular results suggests that continuous fluorescence is not a major effect. An approximate calibration of the

photographic system by the calibration technique to be described in the next section places a hard upper limit on the fluorescent contribution of $\Phi \leq .3$. Thus, less than 30% of the nebular surface brightness can be attributed to continuous fluorescence, based on the results of the photographic spectrophotometry.

It was remarked above that all nebular and control observations gave the same indication except for NGC7023, which gave a very strong, but equally false, indication of fluorescence. The reason for this is that the illuminating star is an emission line star with a variable spectrum. At the time of these observations the stellar lines were quite deep and the nebular spectrum was nearly featureless. However, for more than a year before these observations, the stellar spectrum was also nearly featureless as a result of emission filling in the Balmer lines. Due to the finite velocity of light this latter spectrum was still being reflected by the nebula.

IV. The Photoelectric Observations

In order to eliminate some of the problems intrinsic to photography, it was decided to search for a possible continuous fluorescence component in reflection nebulae by photoelectric techniques employing pairs of wide and narrow interference filters having peak transmissions at the same wavelength centered on prominent absorption lines. The continuum intensity is determined by using the wide band filter and the intensity at the line center is determined by using the narrow band filter. Both star and nebula were observed through both the wide and narrow filters. Again, continuous fluorescence will manifest itself in that the line will appear to be deeper in the star than in the nebula.

The observations were made during three periods: between September 12 and 19, 1971; between November 9 and 15, 1971; and between January

12 and 19, 1972. The photometer used was a 1P21 tube with a single channel pulse counting circuit at the f/13.5 focus of the Kitt Peak National Observatory's No. 1-36" reflecting telescope. A circular diaphragm corresponding to 75 arc seconds was used for nebular observations and a 21 arc second diaphragm was employed for stellar observations. The filters were designed for study at the lines H_β and H_δ(λ=4861Å and 4102Å, respectively).

The amount of fluorescence present can be determined quantitatively as follows: define a parameter x by

$$x = \frac{N_n}{W_n} \cdot \frac{W_s}{N_s} \cdot \tag{2}$$

Here W and N are observed count rates for the wide and narrow filters, respectively, and the subscript s or n indicates whether the observation is stellar or nebular. Equation (2) may only be employed after all observational corrections have been applied. Calibration of the system was carried out by noting that

$$N_s \propto \int_0^\infty I(\lambda)\, T_N(\lambda) d\lambda \tag{3}$$

where $I(\lambda)$ is the intensity of the star's light as a function of λ and $T_N(\lambda)$ is the transmission of the narrow filter as a function of λ. A similar relationship holds between the wide filter count rate, W_s, and the wide filter transmission profile $T_W(\lambda)$. In practice, $I(\lambda)$ was determined from the photographic stellar spectrograms and the transmission functions were provided by filter manufacturers. Note that if a continuous fluorescence, Φ, is present, where Φ is measured in units of intensity in the continuum, equation (3) becomes

$$N_n \propto \int_0^\infty [I(\lambda)+\Phi]T_N(\lambda)d\lambda.$$

Again, a similar expression holds for W_n. Thus, by assuming a series of values of Φ and using the observed $I(\lambda)$ and $T(\lambda)$ functions, it was possible to use equations (2) to (4) to compute x as a function of Φ. Integrations were performed numerically with steps of 1.3Å. The results of these computations are shown in Figure 4 for the H_δ filter pair.

Nebulae to be observed were selected from Cederblad's (1946) catalog. Selection criteria required that the illuminating star be of spectral type A or late B, single, and in an area relatively free of background stars. Preference for inclusion was given to nebulae which overstep the Hubble relation. In addition, one observations control (15 Sextantis) was included. Instrumentally scattered light from this A-type star was treated and reduced as if it were nebular light. This should insure that there is nothing in the technique which gives a false indication of fluorescence. Nebulae which were observed and details of the observations are given in Table II. Also, see Figure 5, 6, 7, and 8.

V. Corrections

The major corrections which are required are

a) Corrections for night sky brightness
b) Correction for scattered light from the illuminating star
c) Correction for contamination of the stellar observation by nebular light
d) Corrections for dead time when bright stars are observed

a) The Night Sky Correction

In principle, the contribution of night sky brightness to the observed count rate can be removed by subtracting the observed count rate for the night sky as observed at a region free of stars or nebulosity.

In practice, two difficulties arise: first, the sky background may change over short time periods and second, it is not always easy to decide which region of the sky is "typical" due to the frequently complex structure of regions surrounding reflection nebulae.

During each observing night, the sky background was monitored to determine the time scale of fluctuations and integration times were kept shorter than typical sky fluctuation times. Integrations through the wide filter were 50 seconds in duration, while narrow filter times varied between 50 and 450 seconds, depending on the constancy of the sky background. The star was observed through the wide and narrow filter at the beginning and end of each run and at intervals of 30 to 45 minutes. After the initial stellar observation, the sky was observed through both filters, then the nebula, then the sky again. For each nebular observation the sky correction was taken to be the average of the previous and subsequent sky observations.

The most difficult aspect of the sky correction is selecting a sky point which is typical. In the case of IC1287 the decision is easy, for the edge of the nebula is well defined. (See Figure 5). In complex regions such as near NGC1435 and NGC2068, selecting a region which is completely free of nebulosity entails the risk of failing to correct for foreground material. Since it is not known whether surrounding nebulosity is foreground or background material, it is necessary to make an assumption on this question and to see how changing this assumption alters the results.

Figure 6 shows NGC1435 and two regions, s and s' selected for sky background observations. Region s' was chosen assuming that it represents typical foreground material. Dr. Conrad C. Dahn, of the U.S. Naval

Observatory, was kind enough to draw our attention to the particular clear patch of sky near BD+22°532. Data reduced using s' as the sky point produced x values less than unity. Since it is difficult to imagine a physical mechanism which could cause this, region s was chosen for sky background measurements. Figure 7 shows the regions of NGC1435 selected for observation.

Figure 8 shows NGC2068 and the point which was chosen for sky observation. Since the dark lane passing near the star is probably a foreground dust lane, this was chosen as the sky point.

b) The Scattered Light Correction

The importance of scattered light when working at small offsets from stars has been discussed by Elvius and Hall (1966), who examined the dependence of scattered light on offset distance, wavelength, night, and condition of optics. A systematic investigation of scattered light was made during the January observing period, although at least one scattered light run was made during each night of the September and November periods.

Scattered light determinations were made by first observing the star λ Ursae Majoris, then observing a dark sky region 25' from the star, then returning to the star until the original sky position was reached. Finally, the star was remeasured. To eliminate any systematic effects, some scattered light runs were made in the opposite direction and some were made by skipping around from one offset to another. No significant difference appeared when results of these different procedures were compared. All scattered light observations were made through the wide filter and typically required 40 to 50 minutes. Scattered light observations were reduced by subtracting the large offset sky values (which included dark current)

from the smaller offset observations. These scattered light values were then normalized to the average of the star count rates.

The surprising result of this investigation of scattered light is that the correction appears to be independent of all the parameters which were considered. Figure 9 shows data for several of the scattered light runs. Notice that there is no significant difference from night to night. Also note that H_β and H_δ lie along the same curve and that it does not matter if the run is along a direction in which a secondary support diffraction spike lies (N-S) or between such spikes. The large diaphragm (2.5mm) used here may be important in interpreting this result. Hour angle does not affect the result either, as determined by making scattered light runs beginning at hour angles of 4 hours east and of 45 minutes east. Attempts to fit scattered light observations to various functional forms met with little success. The large offset at which scattered light is found is surprising.

In practice, the scattered light correction for any nebular observation was made by multiplying the normalized correction factor as read from Figure 9 by the count rate for the illuminating star.

c) The Finite Diaphragm Correction

The third correction which must be considered is the possible contamination of the stellar photometry by inclusion of nebular light. This would result in an underestimate of any fluorescence because stellar lines would appear filled in by additional continuous fluorescence. Only in the case of a faint star and a bright nebula, such as NGC2068, does this effect become important. A series of runs was made in which the illuminating star was observed through a series of diaphragm sizes. Letting ρ denote

the observed count rate, s denote the stellar contribution to ρ, A be the diaphragm area, and B be the surface brightness of the nebula in rate per unit area,

(5) $$s = \rho - BA,$$

assuming a uniform surface brightness. To determine the true stellar count rate through each filter, one simply fits the observed count rate as a function of diaphragm area to the form of equation (5) and extrapolates to zero diaphragm area.

d) Dead Time

Observations of brighter stars had to be corrected for dead time of the photon counting system. If ρ is the observed count rate, the true count rate, ρ_o, is

$$\rho_o = \rho\left(1+\frac{\rho}{20\times10^6}\right)$$

The numerical value was provided by Jeanette Barnes of the Kitt Peak Staff.

VI. Photoelectric Results

The results of the observations are displayed in Table II . The first column lists the nebula, the second gives the wavelength at which observations were made, the third indicates the position in the nebula (see Figures 7 and 8). The fourth and fifth columns give the offsets from the illuminating star at which the nebula was observed. The next column is the average value of x obtained and σ is the rms deviation of the individual observations from the quoted result. The column marked t is the total number of seconds spent observing the nebula through the narrow band filter. Time spent on determining the sky correction and making observations which were ultimately rejected is omitted from this number.

Inspection of the results presented in Table II immediately indicates that there is no evidence for fluorescence to the accuracy with which it can be detected by this technique. All of the values determined for x are within one standard deviation of unity except for the NGC2068 results, which are systematically too low.

The low x values for NGC2068 are probably due to the presence of a faint star which was impossible to exclude from the field of view of the photometer during observation of the illuminating star. This star is about 1.5 magnitudes fainter than the illuminating star and about 5" east of it.

For the best determined case, that of NGC1435, $x=1.00\pm.02$ is a reasonable summary of the observational results. Consulting Figure 4, we see that an rms deviation of .02 in R corresponds to an uncertainty of about .1 in Φ. Thus, if continuous fluorescence is present, it accounts for less than 10% of the total surface brightness in this nebula. The fact that little or no continuous fluorescence is observed in reflection nebulae can serve to eliminate from further consideration any particle model which predicts such fluorescence. This criterion, however, constitutes a rather insensitive test for discriminating between such models.

VII. Conclusions

Photoelectric photometry and photographic spectrophotometry indicate that little or no continuous fluorescence occurs in the reflection nebulae which were observed. We conclude that fluorescence is not likely to be the reason that reflection nebulae have indicated generally high values

of albedo. A more thorough discussion of the surface brightness of reflection nebulae is therefore in order.

In addition, the spectrophotometry did not show any indication of the presence of any diffuse interstellar features, such as the feature at 4430Å.

Finally, observers planning future work comparing nebular spectra with spectra of the illuminating stars should be careful to avoid cases such as NGC7023, in which the stellar spectrum is variable.

Acknowledgements

Helpful discussions with Dr. Conrad Dahn and Dr. C. R. O'Dell are gratefully acknowledged. We would also like to thank Dr. O'Dell for his permission to use the Yerkes Observatory's microdensitometer. Funds provided by NASA grant No. NGR36-010-016 are much appreciated, as are travel funds provided by AURA and The University of Toledo. Finally, we would like to thank the staff of the Kitt Peak National Observatory for their enthusiastic and helpful support.

TABLE I NEBULAR EXPOSURES

OBJECT	DATE	EXPOSURE TIME (MINUTES)	SLIT ORIENTATION
NGC1435 (Merope)	9/27/70	60	NS
	9/28/70	90	NS
	9/29/70	60	NS
	12/29/70	60	NS
	12/30/70	60	NS
	12/31/70	60	NS
NGC2068	9/27/70	60	EW
	9/29/70	75	NS
	12/30/70	90	NS
	12/31/70	90	NS
	1/1/71	90	NS
NGC7023	9/27/70	60	EW
	9/29/70	120	EW

TABLE II RESULTS OF THE PHOTOELECTRIC OBSERVATIONS

OBJECT	λ(Å)	POS.	NS(')	EW(')	X	σ	t(sec)
IC1287	4102		2.7 S	2.2 W	1.026	.066	2750
NGC1435	4861	2	1.9 S	1.9 W	.997	.020	1750
"	"	1	10.5 S	1.9 W	.971	.013	1750
"	4102	2	1.9 S	1.9 W	1.017	.023	5150
"	"	1	10.5 S	1.9 W	.984	.029	7050
NGC2068	4861	1	0.0	1.0 E	.974	.014	1750
"	"	2	1.0 S	1.0 E	.981	.012	1250
"	"	3	2.5 S	0.0	.941	.005	500
"	4102	1	0.0	1.0 E	.937	.015	4500
"	"	2	1.0 S	1.0 E	.944	.020	3500
"	"	3	2.5 S	0.0	.946	.015	1750
15 Sext	4102		1.3 S	1.3 W	1.015	.010	2450

REFERENCES

Aller, L. H., 1956, Gaseous Nebulae, John Wiley & Sons, Inc.

Becker, R. S., 1969, Theory and Interpretation of Fluorescence and Phosphorescence, Wiley Interscience.

Blair, I. M., and Edgington, J. A., 1968, Nature, 217, 157.

Cederblad, S., 1946, Lunds. Obs. Med., Ser II, No. 119.

Elvius, A., and Hall, J. S., 1966, Lowell Obs. Bull., 6, 257.

Grainger, J. F., and Ring, J., 1969, Physics and Astronomy of the Moon, ed. by A. Kopal, Academic Press, New York.

Link, F., 1961, in Physics and Astronomy of the Moon, ed. by A. Kopal, Academic Press, New York.

Struve, O., and Swings, P., 1948, P.A.S.P., 60, 61.

Figure Captions

Figure 1. The effect of an additional continuous fluorescent component is to alter the apparent line depth of a spectral feature. The reflected component (solid line) and the fluorescent component (dotted line) add to give the observed spectrum (broken line).

Figure 2. A peak in the plot of R as a function of wavelength would normally suggest the presence of continuous fluorescence. However, these data for NGC1435 give a false indication of fluorescence, due to the photographic effect discussed in section III.

Figure 3. The false indication of fluorescence originates in the non-linearity of the photographic characteristic curve (A) at low light levels. As one moves farther from the star (see B), nebular intensity decreases in both line and continuum proportionally, but non-linearity causes the line to appear filled in at larger r (C).

Figure 4. The amount of fluorescence, Φ, in units of the continuum, can be determined knowing the observationally determined parameter, x.

Figure 5. The nebular and sky observation points for IC1287 are shown on the blue print of the Palomar Sky Survey. The size of the circles indicates the area observed.

Figure 6. The sky observation s and s' points for NGC1435 are shown on the blue print of the Palomar Sky Survey.

Figure 7. The nebular observation points for NGC1435 are shown here on the blue print of the Palomar Sky Survey.

Figure 8. The nebular and sky observation points for NGC2068 are shown here on the blue print of the Palomar Sky Survey. The white dot is the point of the illuminating star.

Figure 9. Scattered light (normalized to stellar count rate) is shown as a function of offset angle. Note the independence of results on date, wavelength, and direction.

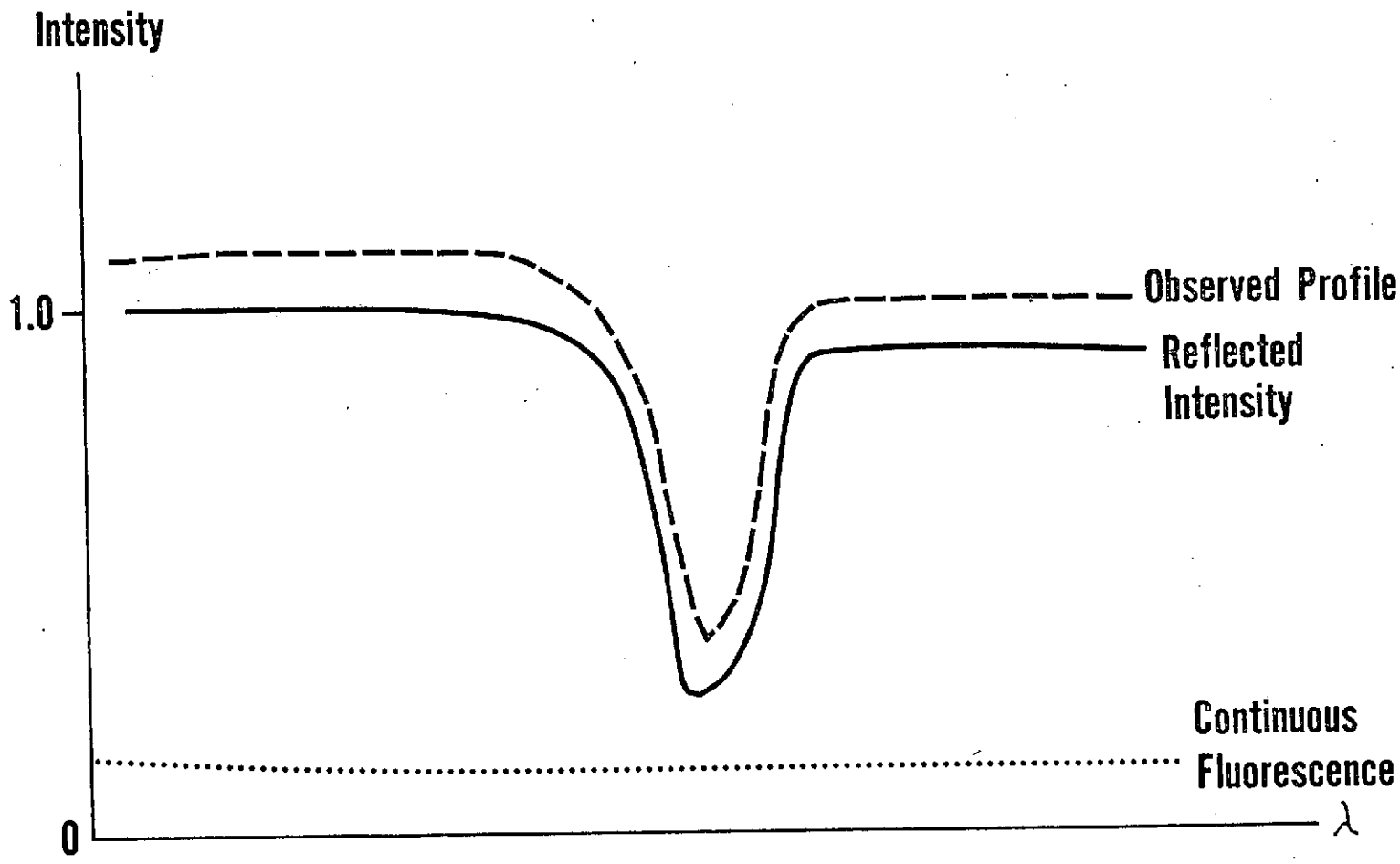
Intensity
1.0
0
Observed Profile
Reflected
Intensity
Continuous
Fluorescence
λ

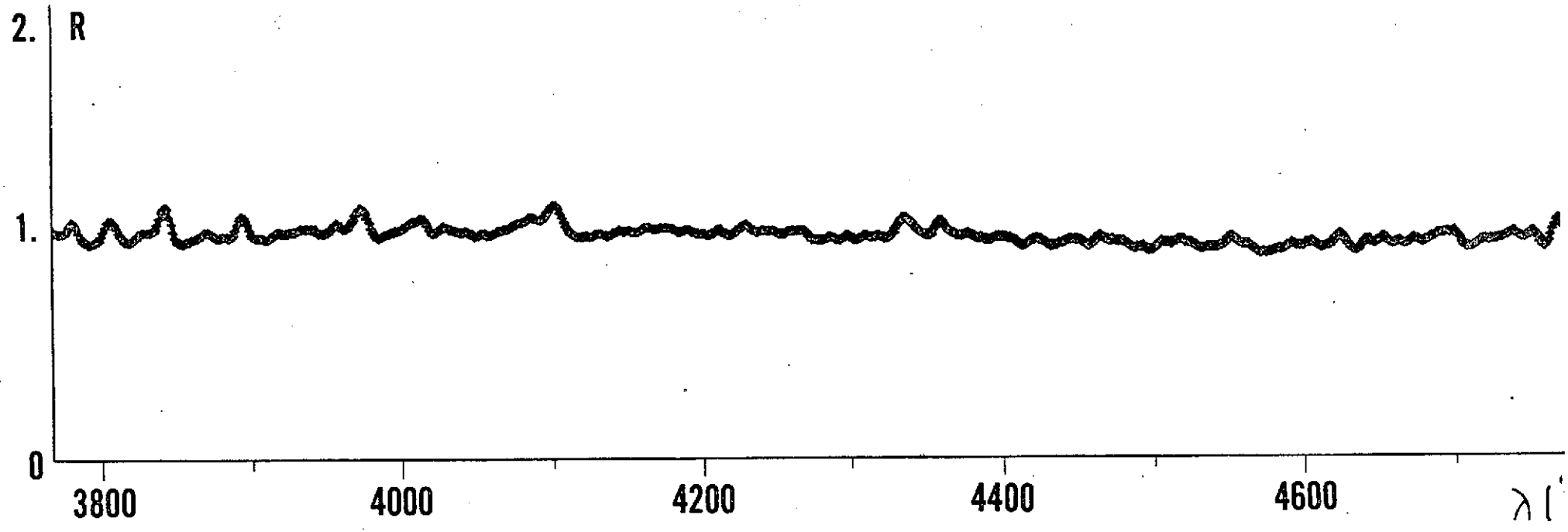
2.
R
1.
0
3800
4000
4200
4400
4600
λ (

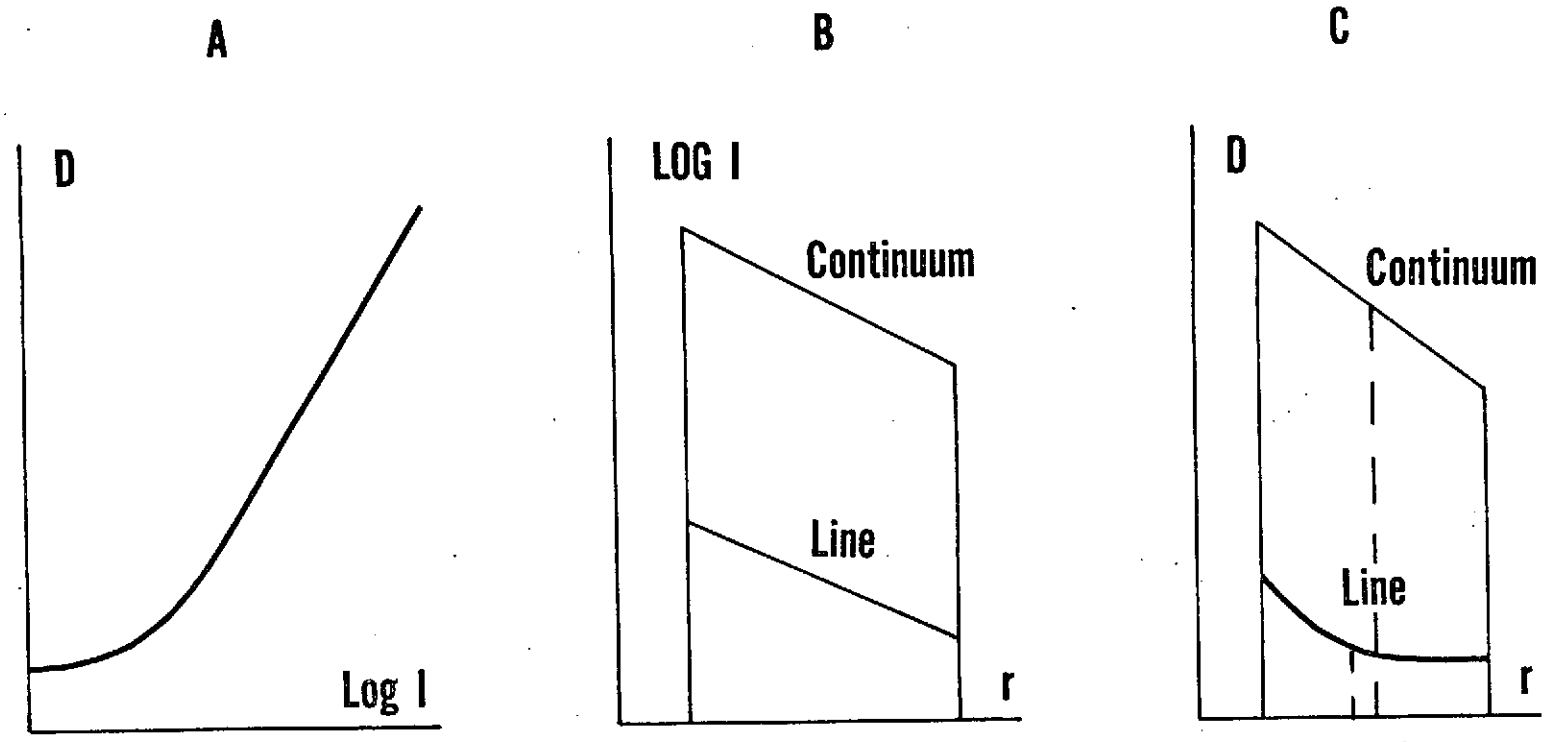
A
D
Log I
B
LOG I
Continuum
Line
r
C
D
Continuum
Line
r

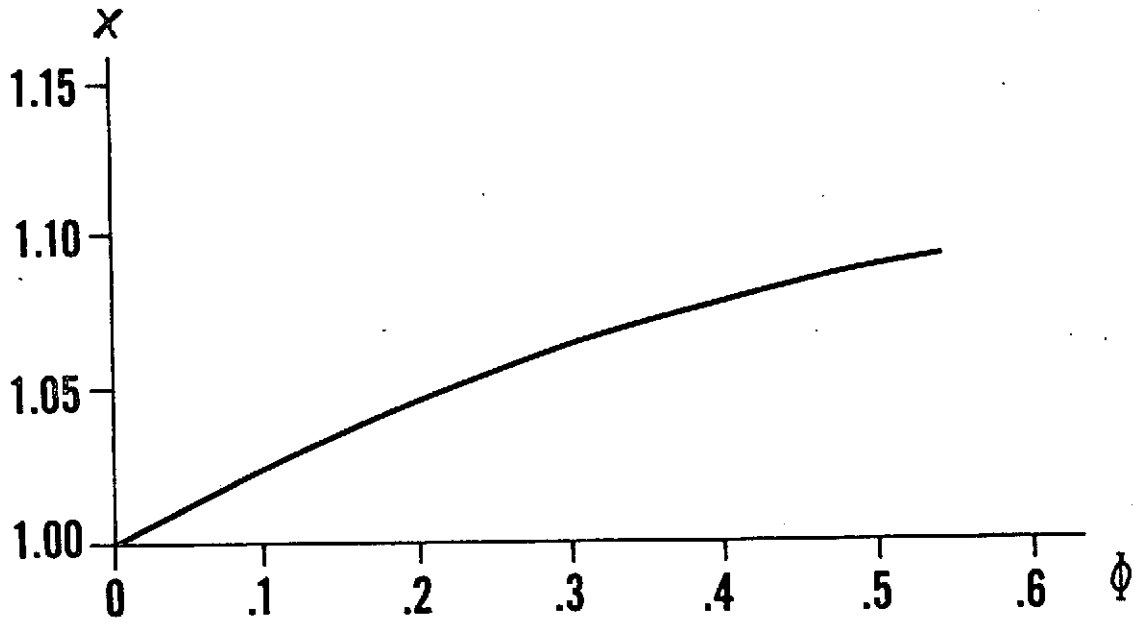
X
1.15
1.10
1.05
1.00
0
.1
.2
.3
.4
.5
.6
Φ

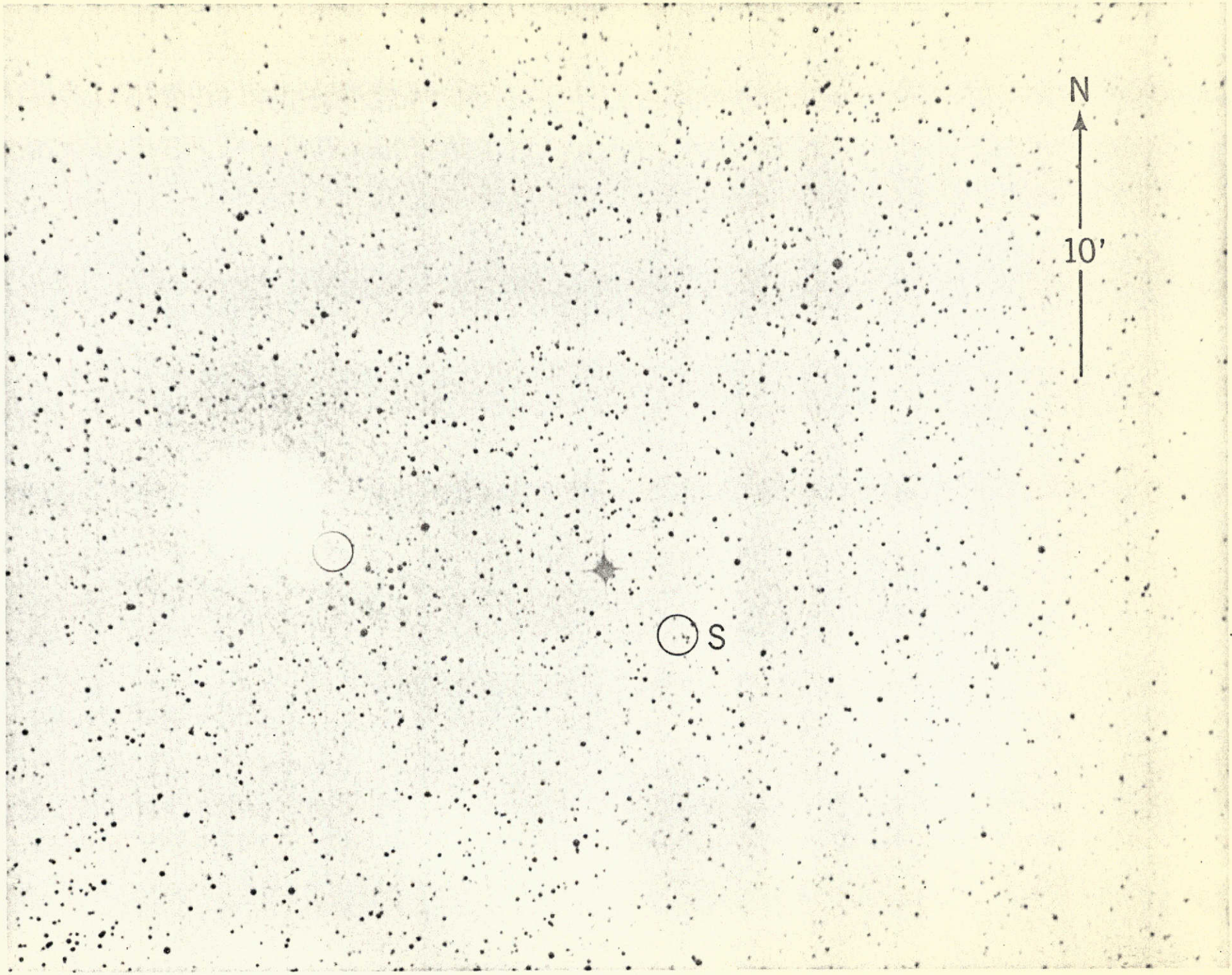
N
10'
S

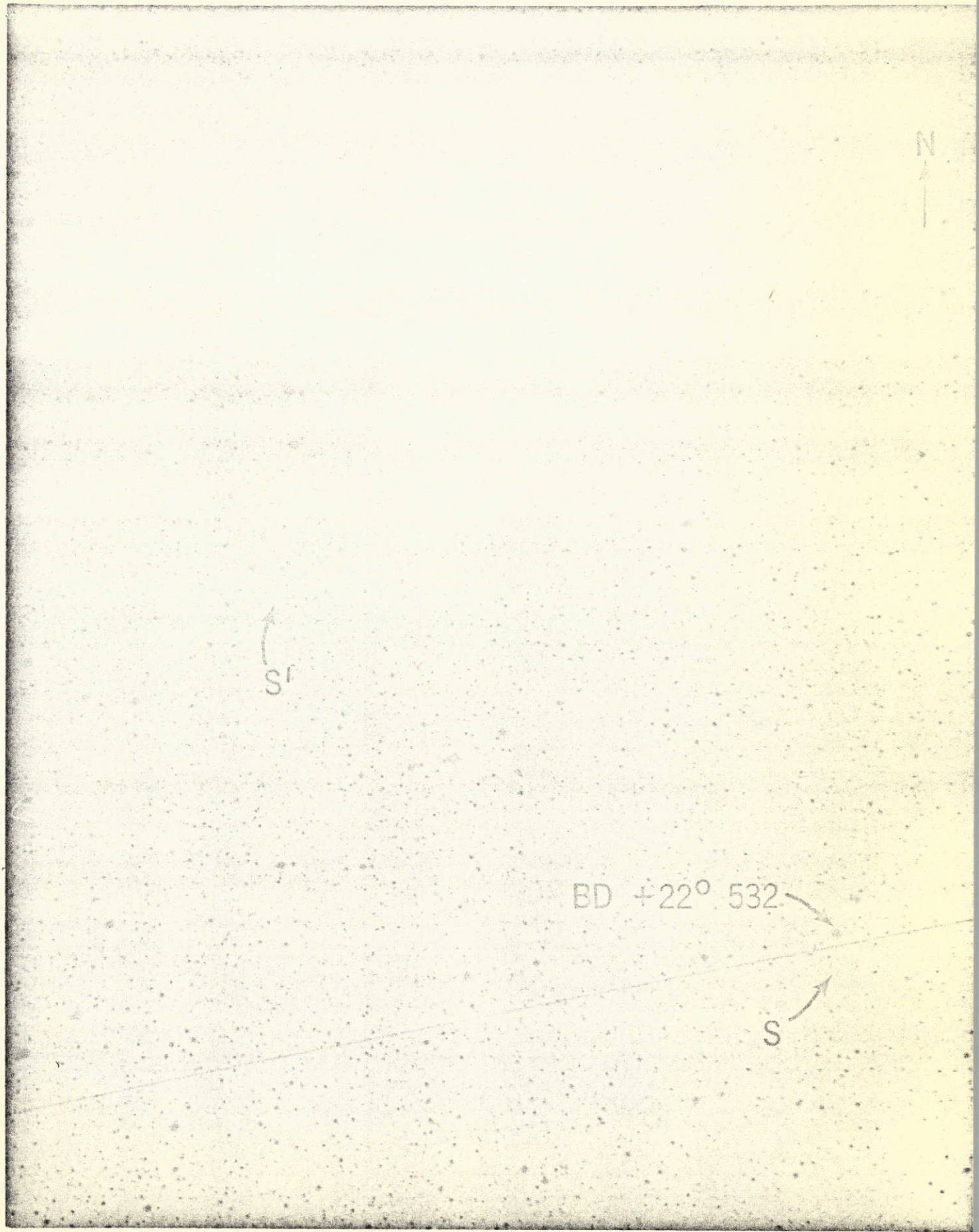
N
S'
BD +22° 532
S

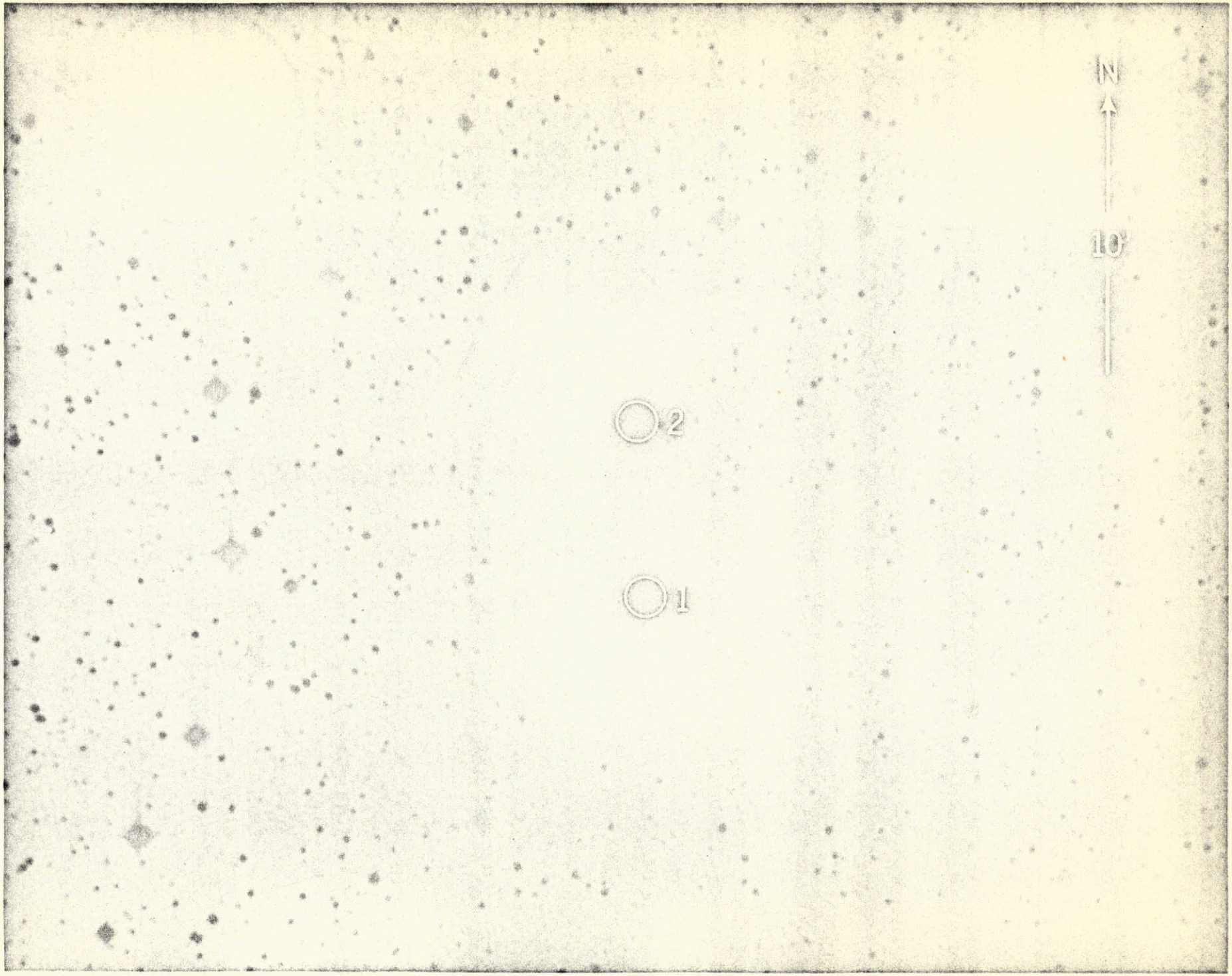
N
10'
2
1

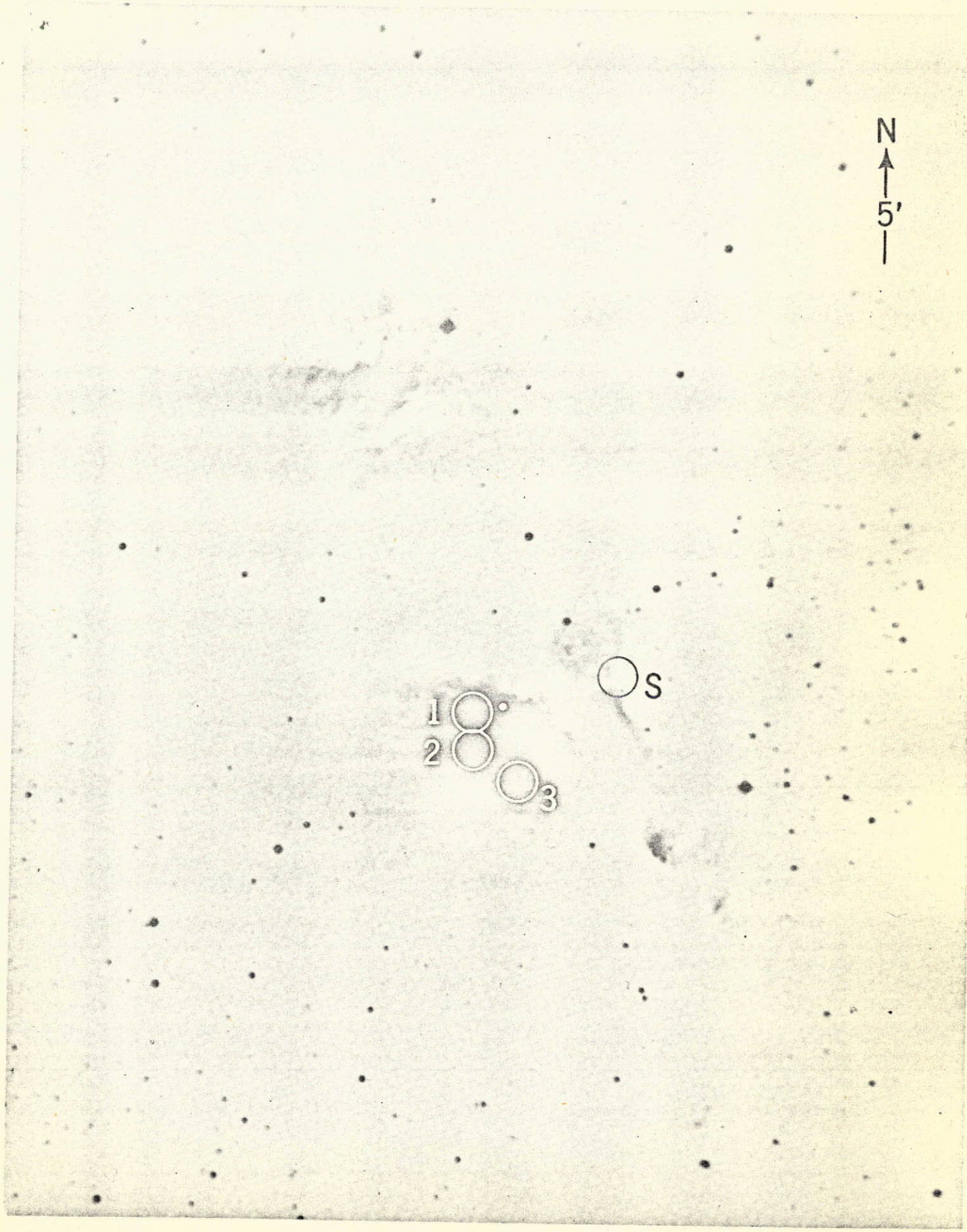
N
5′
S
1
2
3

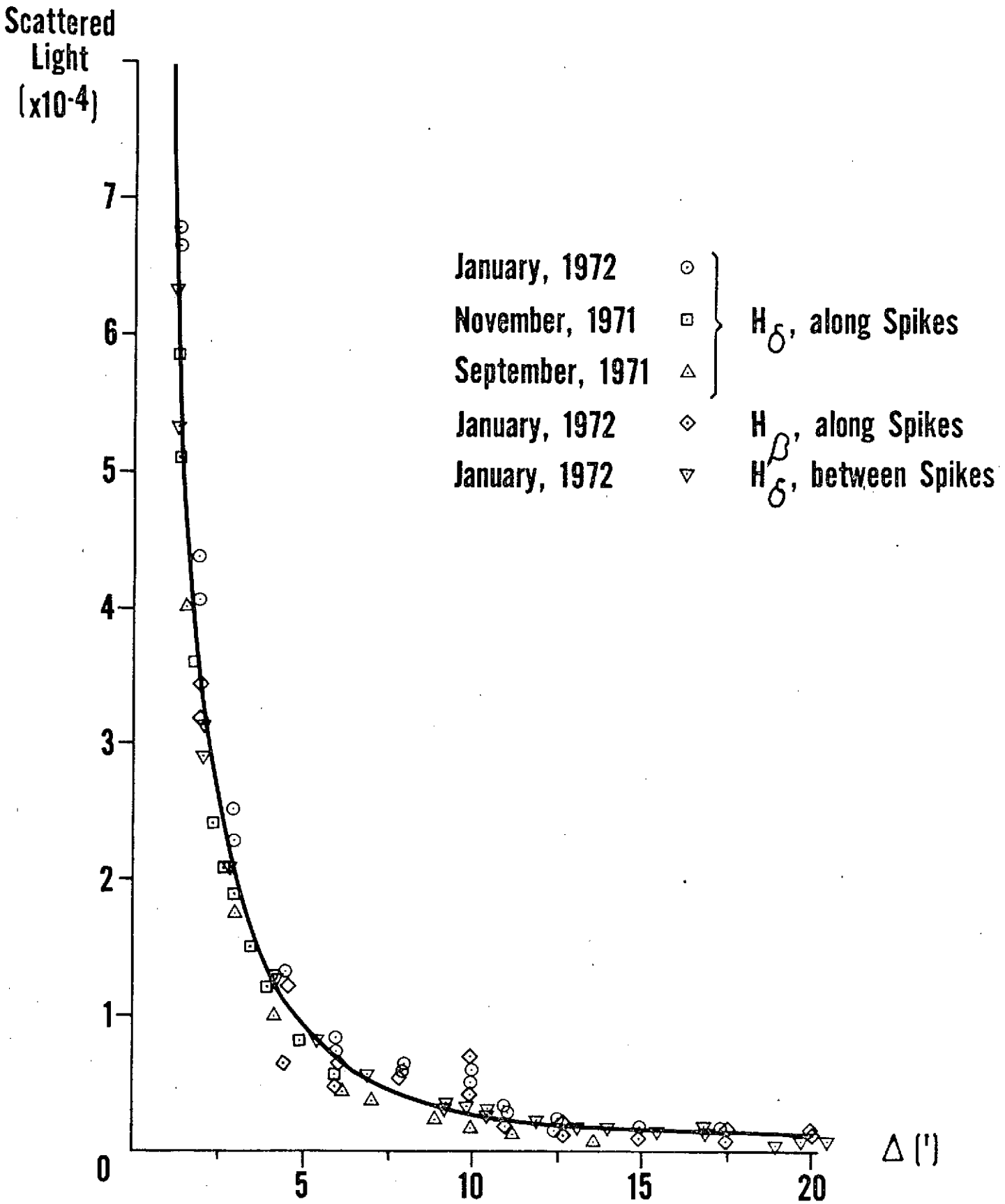
Scattered Light (x10-4)
7
6
5
4
3
2
1
0
5
10
15
20
Δ (')
January, 1972
November, 1971
September, 1971
Hδ, along Spikes
January, 1972
Hβ, along Spikes
January, 1972
Hδ, between Spikes